Upconversion Luminescence of β-$NaYF_4$: Yb^{3+}, Er^{3+}@β-$NaYF_4$ Core/Shell Nanoparticles: Excitation Power Density and Surface Dependence

Yu Wang,[†,‡,§] Langping Tu,[†,‡,§] Junwei Zhao,[†,‡] Yajuan Sun,[†] Xianggui Kong,*[,†] and Hong Zhang*[,§]

Key Laboratory of Excited-State Processes, Changchun Institute of Optics, Fine Mechanics and Physics, Chinese Academy of Sciences, 16 Eastern South Lake Road, Changchun 130033, P. R. China, Graduate School of Chinese Academy of Sciences, Beijing 100039, P.R. China, and Van't Hoff Institute for Molecular Sciences, University of Amsterdam, Nieuwe Achtergracht 166, 1018 WV Amsterdam, The Netherlands

Received: January 13, 2009; Revised Manuscript Received: February 19, 2009

Coating a homogeneous layer outside the core nanoparticles has become a common method to improve the optical properties of nanoparticles. For rare earth ion-doped nanoparticles, although the homogeneous coating is found to enhance the upconversion luminescence, a large deviation in the reported enhancement amplitude, however, demonstrates the lack of a complete picture of the enhancement mechanism. In this work, we have performed steady-state and time-resolved spectroscopic studies on one of the most efficient upconversion nanosystems − β-$NaYF_4$:Yb^{3+},Er^{3+} and β-$NaYF_4$:Yb^{3+},Er^{3+}@β-$NaYF_4$ core/shell nanoparticles. Roles of the surface quenching centers, typically the high-frequency vibrational modes provided by the organic surfactants in the upconversion luminescence, are studied in detail. Our results show that excitation power density, once over a threshold, say ~150 W/cm^2 in this case, does have a non-negligible annealing effect, which may even lead to high luminescence upconversion intensity of the core nanoparticles compared to the shell-coated nanoparticles. The surface-related high-frequency vibrational modes play an important role in the upconversion process and in the laser annealing process, and the latter manifests itself in the difference of the laser annealing effect between the core and core/shell nanoparticles. From the upconversion luminescence kinetics analysis, it turns out that the luminescent centers of the core nanoparticle are severely quenched but homogeneous coating can effectively reduce the quenching, enhancing the upconversion luminescence. It is concluded that the upconversion emission spectrum, or more specifically the ratio between the red and green emissions, can be greatly altered by excitation power density for core nanoparticles but not for core/shell nanoparticles.

Introduction

In recent years, upconversion nanoparticles have attracted much attention because of their superior spectroscopic properties, which may lead to a great deal of potential in many fields, especially in biology/biomedicine.[1−6] Among other advantages, the excitation can be realized by a compact, high-power, and inexpensive diode laser at near-IR, for example 980 nm, within the optimal optics window of human tissues. In these biomedical applications, upconversion efficiency is of critical importance because the sensitivity of labeling or efficacy of therapy relies on the luminescence of individual nanoparticles.

Hexagonal-phase sodium yttrium fluoride (β-$NaYF_4$), known as one of the most efficient host materials ever,[7,8] has been widely studied recently.[9−18] In bulk, the low phonon energy of the host strongly suppresses multiphonon relaxation process in the emission centers, leading to a strong green upconversion emission ($^2H_{11/2}$, $^4S_{3/2} \rightarrow {}^4I_{15/2}$) and a very weak red upconversion emission ($^4F_{9/2} \rightarrow {}^4I_{15/2}$) at low doping level, because of the feeding of $^4F_{9/2}$, of which the red upconversion emission comes, requires phonon assistance to bridge the gaps on the order of several thousand cm^{-1}, which cannot be efficiently bridged by the phonons of the host lattice, being on the order of several hundred cm^{-1}. When the size of the crystal decreases to the nanometer level, it is generally observed that the red upconversion emission versus the green one is (much) stronger than their bulk counterpart, which is usually ascribed to the existence of high vibrational frequencies, provided by organic surfactant molecules, such as −OH, −CH, and so forth, which are comparable to the energy gaps of the emission centers.[19−21] However, the underlined mechanism is still very vague.

To enhance the emission core/shell structure has been generally adopted for nanoparticles including rare earth ion-doped nanocrystals with the hope that the surface, hence the quenching centers, would be separated in space from the emission centers. In reality, both homogeneous and inhomogeneous core/shell structures have been synthesized and examined.[22−32] Typically, a homogeneous core/shell structure is favorable because this design can reduce the lattice mismatch between the core and the shell. Indeed enhancement of luminescence and upconversion has been observed from the core/shell nanoparticles.[14,32] The factor of enhancement is often given based on the experimental results under relatively high excitation radiation, without taking into account the possible laser-induced annealing.[33] Besides, the annealing dynamics should be related to the surface-related vibrational properties because the annealing process is basically thermodynamic in nature.

* To whom correspondence should be addressed: E-mail: xgkong14@ciomp.ac.cn and h.zhang@uva.nl.
† Chinese Academy of Sciences.
‡ Graduate School of Chinese Academy of Sciences.
§ University of Amsterdam.

10.1021/jp9003399 CCC: $40.75
Published on Web 04/07/2009

The situation introduced above encourages us to perform the present research in order to illustrate the influence of the excitation power density and the surface properties on the upconversion dynamics of the rare earth ions doped in the nanoparticles, employing β-$NaYF_4$:Yb^{3+},Re^{3+} nanoparticles and β-$NaYF_4$:Yb^{3+},Re^{3+}@ β-$NaYF_4$ core/shell nanoparticles. Our results demonstrate that excitation power, once over ~150W/cm^2 in this case, does have a non-negligible annealing effect on the luminescence upconversion dynamics. Also, enhancement of the emission arising from the core/shell structure would be largely exaggerated if this laser-induced annealing effect were not taken into account. In our case, the luminescence upconversion intensity of the core can even exceed that of the core/shell ones, subject to the excitation power density at 980 nm. This unusual behavior is related to the high-frequency vibrational modes of the organic surfactant molecules, which contribute to the upconversion processes differently in the core and core/shell nanoparticles. From luminescence kinetics analysis, it turns out that the luminescent centers severely quenched in the core nanoparticle can indeed be recovered by the homogeneous coating and the recovery effect depends on the shell thickness. It is concluded that the upconversion emission spectrum, for example the ratio between the red and green emissions, can be greatly altered by excitation power density for core nanoparticles but not for core/shell nanoparticles.

Experimental Section

1. Reagents. Rare earth oxides (RE = Y, Yb, Er), oleylamine (OM, >80%, Acros), oleic acid (OA, 90%), octadecene (ODE, 90%, Acros), trifluoroacetic acid (99%, Acros), CF_3COONa (>97%, Acros), ethanol, chloroform, and hexane of analytical grade were purchased from Beijing Chemicals (Beijing, China) and used without further purification. Water used in the experiment was purified to resistivity of 18.2 MΩ.

2. Synthesis of β-$NaYF_4$: Yb^{3+}, Er^{3+} Nanoparticles and β-$NaYF_4$: Yb^{3+}, Er^{3+}@β-$NaYF_4$ Core/Shell Nanoparticles. The synthesis basically followed the routes previously reported in literature.[9,14,34] Briefly, rare earth trifluoroacetates ($(CF_3COO)_3RE$) were prepared at the beginning by dissolving rare earth oxides in trifluoroacetic acid (CF_3COOH), followed by drying at 60 °C. Sodium trifluoroacetate was prepared from sodium carbonate in a similar way. A mixture of a designated molar ratio of $(CF_3COO)Na$ (2 M), $(CF_3COO)_3Y$ (0.78 M), $(CF_3COO)_3Yb$ (0.2 M), and $(CF_3COO)_3Er$ (0.02 M) powder were dissolved in 10 mL oleylamine (OM) and then filtered to get rid of the residues. Under vigorous stirring in a three-neck flask, the mixture was then heated to 110 °C under the protection of nitrogen or argon atmosphere and maintained at the same temperature for 30 min to remove the oxygen and residual water. At this end, the solution was totally clear with a slight yellow color. The mixture was then heated slowly to 300 °C in the presence of argon atmosphere. After 30 min, 5 mL of the core product was taken out for reference. The reaction of the rest was continued for another 30 min with the slow addition of the shell precursors' solution containing $(CF_3COO)Na$ (1 M), $(CF_3COO)_3Y$ (0.5 M) in 5 mL OM. The final mixture was cooled down rapidly to room temperature. Both nanoparticles were then precipitated using ethanol and isolated via centrifugation for at least three times. The resulting nanocrystals were dried in vacuum at 60° for a minimum of 24 h.

3. Setups. XRD studies were performed on powders using a Japan Rigaku D/max-rA X-ray diffractometer system with monochromatized Cu Kα radiation (λ = 1.5418 Å). The upconversion emission spectra were acquired using a Jobin-Yvon LabRam Raman spectrometer system equipped with holographic gratings of 1800 and 600 grooves/mm resolution respectively and a Peltier air-cooled CCD detector. A 980 nm laser diode was used as the excitation source and the beam was either focused (about 8 cm focal length) to a spot size of approximately 0.2 mm in diameter to reach high excitation density or defocused to allow low density excitation. The upconversion luminescence kinetics was recorded with a 500 MHz Tektronix digital oscilloscope and the excitation was realized by a nanosecond pulse train at 980 nm from an optical parametric oscillator. Precise control of sample temperature (0.1 °C) was achieved by means of a Linkam THMS600 temperature-programmable heating/cooling microscope stage. The THMS stage was used in conjunction with a Linkam LNP cooling system when cooling. In the excitation power-dependent upconversion luminescence experiments, the power density increased step by step and the collection time is around 30 s.

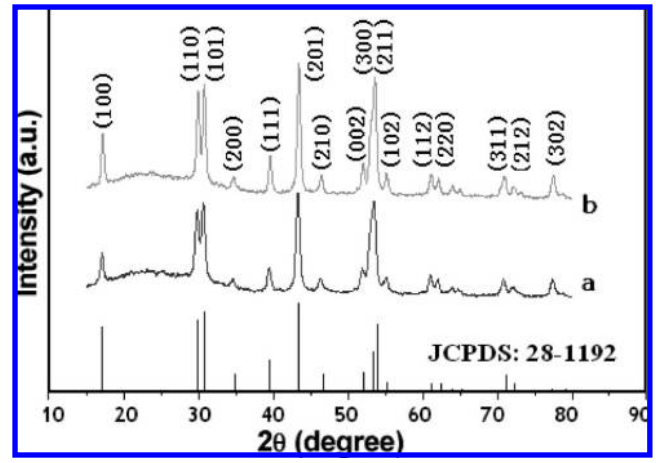

Figure 1. XRD patterns of β-$NaYF_4$: Yb^{3+}, Er^{3+} (a) and β-$NaYF_4$: Yb^{3+}, Er^{3+}@ β-$NaYF_4$ core/shell (b) nanoparticles.

Results and Discussion

1. Characterization. The powder X-ray diffraction (XRD) patterns (Figure 1) of the samples show well-defined peaks, indicating the high crystallinity of the synthesized core and the core/shell structure nanoparticles. The diffraction peaks of β-$NaYF_4$: Yb^{3+}, Er^{3+}@β-$NaYF_4$ core/shell structure nanoparticles are slightly narrower than the XRD pattern of the core. Their peak positions and intensities of the XRD patterns match closely with that of hexagonal β-$NaYF_4$ in *JCPDF* (28−1192). From the line broadening of the diffraction peaks, the crystallite sizes of the samples are estimated to be approximately 13.9 nm for the core and 17.2 nm for the core/shell nanoparticles respectively based on the Debye−Scherrer formula. The volume ratio of the core and core/shell nanoparticles is about 1:1.9, which is consistent with the molar ratio of reaction materials (1:2). The cell parameters of the two samples were calculated by *Unitcell* with the crystal system, peak positions of XRD and corresponding crystal planes: a_c = 5.994 Å, c_c = 3.522 Å for core and $a_{c/s}$ = 5.973 Å, $c_{c/s}$ = 3.518 Å for core/shell nanoparticles, which are somewhat larger than the cell parameters of the bulk β-$NaYF_4$ (a = 5.960 Å, c = 3.510 Å) *(JCPDF 28−1192)*, indicating that shell growing process has improved the crystallinity of the nanoparticles. Large size (~500nm) β-$NaYF_4$ particles were synthesized following the similar route to mimic the bulk situation.

2. Relationship between the Excitation Power Density and Upconversion Luminescence. When the β-$NaYF_4$: Yb^{3+}, Er^{3+} nanoparticles are coated with β-$NaYF_4$ shells, the upconversion

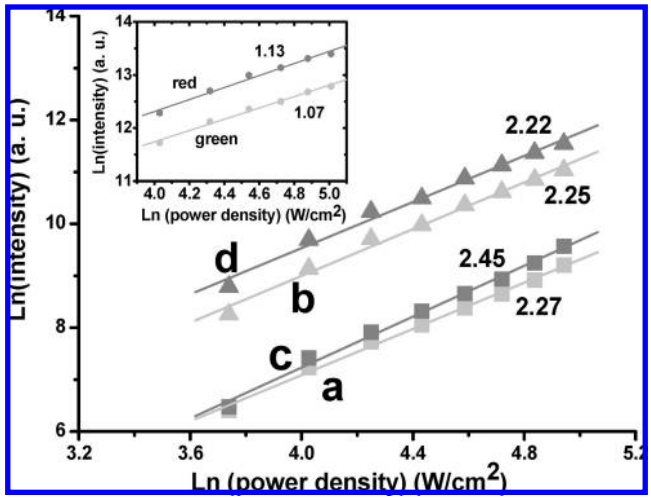

Figure 2. Excitation power density dependence of 525, 545 nm green emissions ($^2H_{11/2}/^4S_{3/2} \rightarrow {}^4I_{15/2}$) of core (a), core/shell (b), and 660 nm red emission ($^4F_{9/2} \rightarrow {}^4I_{15/2}$) of core (c), core/shell (d) at low-power density (<150 W/cm^2). The inset shows excitation power density dependence of green and red emission of the bulk counterpart of size ~500 nm.

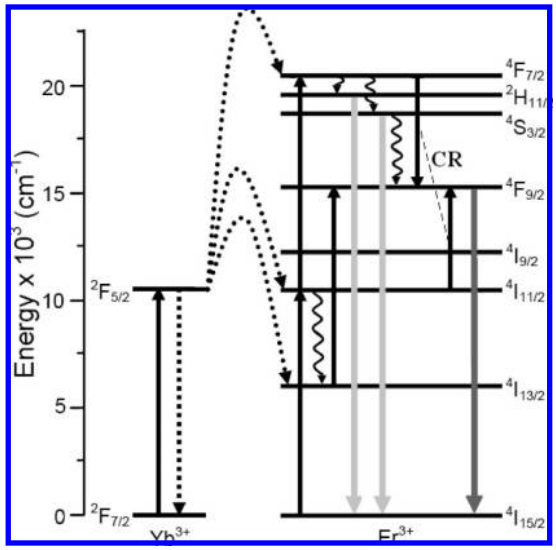

Figure 3. Schematic illustration of the upconversion processes of Er^{3+} in β-$NaYF_4$: Yb^{3+}, Er^{3+} under 980 nm excitation. CR: cross relaxation.

emission intensity is enhanced with respect to that of the core nanoparticles under low excitation power density (Figure 2). Here, low excitation power density is meant for the scenario that in this power region the upconversion spectrum is unique for a specific power density. Usually, this enhancement is attributed to the fact that a significant amount of nonradiative centers located on the surface of β-$NaYF_4$: Yb^{3+}, Er^{3+} nanoparticles are eliminated by the β-$NaYF_4$ shell. On top of that, the distance between the luminescent rare earth ions and the surface quench centers in the core/shell structure is increased, which will reduce the nonradiative transition probabilities as well.

At high Yb^{3+} concentration, the upconversion processes for the red and green emissions are depicted in Figure 3, from which it can be seen that the origin of the red emission is complex; three population routes coexist for the $^4F_{9/2}$ level.

In an upconversion mechanism (ESA or ETU) where linear decay is dominant, the visible output intensity (I_V) will be

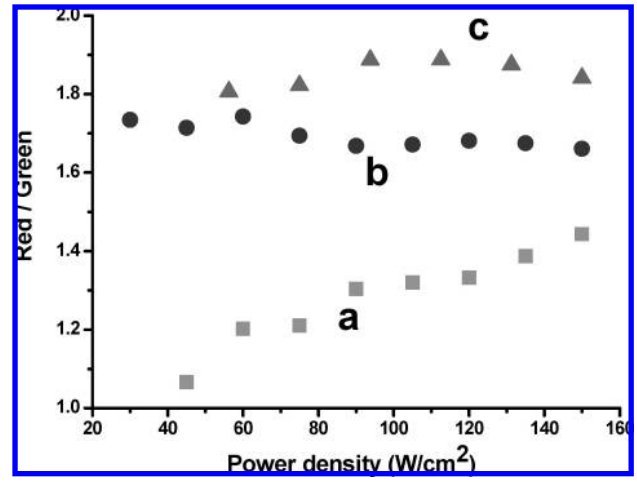

Figure 4. Excitation power density dependence of the intensity ratio of red to green emissions for the core (a), core/shell nanoparticles (b), and bulk counterpart (c).

proportional to some power (n) of the infrared excitation (I_{IR}) power at low excitation power density:[35]

$$I_V \propto I_{IR}^n \quad (1)$$

where n is the number of IR photons absorbed per visible photon emitted.

In our experiments, n varies from 2.45 (core) to 2.22 (core/shell) for the red emission and from 2.27 (core) to 2.25 (core/shell) for the green emission. This phenomenon manifests itself as the involvement of processes other than ETU and/or ESA, which should lead to n being not over 2; considering the relatively high concentration of Er^{3+} (2 mol %) cross relaxation ($^4F_{7/2} \rightarrow {}^4F_{9/2}$ vs $^4I_{11/2} \rightarrow {}^4F_{9/2}$) that should occur here,[36] which might be responsible for the high n. This assignment, however, seems against the observation that, in the core/shell structure, n is closer to 2, especially for the red emission. This concern might be released by the following argument. Compared to the core nanoparticles, the impact of the high-frequency vibrational modes brought in by the surface organic groups will be much less in the core/shell nanoparticles due to the space separation between the vibrational modes and the luminescent centers (vide supra). These vibrational modes are essential for the two population routes of the red emission (Figure 3). Indeed for the bulk counterpart, the upconversion red emission is very weak at low doping levels.[37] However, one should not forget that the relatively high concentration of Yb^{3+} and Er^{3+} causes a non-negligible cross relaxation process here as evidenced by the strong red emission of the bulk sample (Figure 4), where if linear decay of the intermediate state is dominant, $^2H_{11/2}/^4S_{3/2}$ and $^4I_{11/2}$ should experience respectively a quasi-quadratic and a quasi-linear excitation power dependence, and therefore n should be around 3; otherwise n should be less and will reach the minimum when the upconversion, instead of the linear decay, becomes dominant. The former scenario is similar to the case of core nanoparticles when nonradiative vibrational relaxation is very effective, whereas the latter one refers to core/shell nanoparticles where the surface-related high-frequency vibrational modes do not greatly affect the luminescent centers due to the separation of the luminescent centers from the surface. This argument is supported by the fact that n of the red emission is the lowest for the bulk sample (i.e., the one with size of ~500 nm) among the three samples. Note that the cross relaxation is not important for the green emission and thus n does not vary much between the core and core/shell structures. This relationship can be used

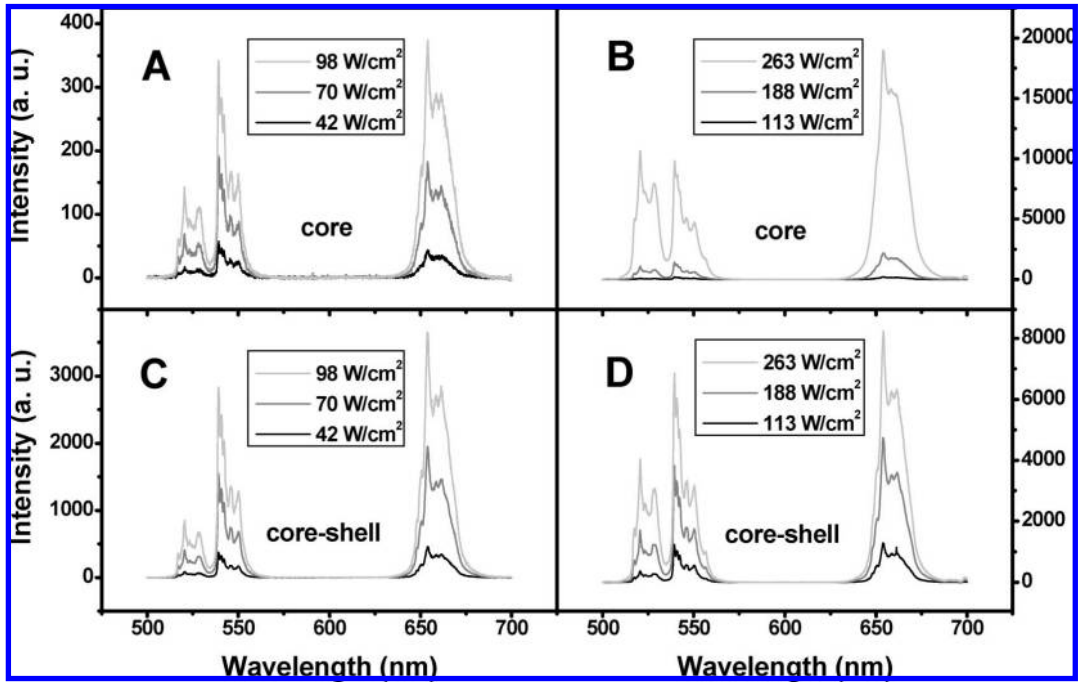

Figure 5. Upconversion spectra of the core (A, B) and core/shell nanoparticles (C, D) under different NIR excitation power density. Here, A and C are measured with the same slit width of monochromator, whereas the slit for B and D is smaller.

to change color of the upconversion luminescence. In Figure 4, the intensity ratio of red to green upconversion emissions demonstrates dependence of the excitation power density and the nanostructure. For core nanoparticles, the ratio is almost 1 at low excitation power density but increases significantly with the excitation power density. This, however, does not happen for core/shell and the bulk samples where the ratio varies only slightly with excitation power density. Therefore, the upconversion emission spectrum can be greatly altered by the excitation power density under the existence of an intermediate level with efficient nonradiative relaxation channels, for example in the case of core nanoparticles.

In the discussion so far, we have not brought the effect of laser-induced thermal effect into consideration. In general, caution must be paid when one tries to assess quantitatively the enhancement of the upconversion luminescence because various factors might contribute to the enhancing mechanism, rather than simply the separation between the surface quench centers and the luminescence centers, for example, excitation power density dependence of the upconversion luminescence, the possible laser-induced annealing, and uneven excited number of the luminescence centers due to the different size between the core/shell and core nanoparticles, which are the ones often neglected in the evaluation.

Highly doped sensitizer Yb^{3+} increases significantly the excitation absorption, which naturally also stimulates the worry of heating effect. To study the excitation power effect, we compare the two scenarios: low excitation power density as we have discussed so far, that is <150 W/cm^2 where the upconversion spectrum can be recovered when the excitation power density decreases back to the low value, and high excitation power density, that is >150 W/cm^2, where the spectrum under lower excitation density cannot be recovered when the excitation power density decreases back.

In Figure 5, the upconversion spectra in the two scenarios are shown for both the core and core/shell nanoparticles. It can be seen that at the lowest excitation power density applied in our experiment the upconversion emission of the core nanoparticles is weaker than that of the core/shell nanoparticles. This trend holds in the whole low excitation power density region but is, however, reversed when the excitation power density is over $\sim$200 W/cm^2 (Figure 6), where upconversion emission is stronger for the core than for the core/shell nanoparticles. The behavior under high excitation power density is apparently related to the annealing effect because the upcoversion spectra of both samples cannot be recovered when the excitation power comes back. Similar observations have been reported.[38,39] To understand the mechanism, we have measured the temperature of the radiation area of the samples. As is well-known, the close-lying $^2H_{11/2}$ and $^4S_{3/2}$ satisfy the Boltzmann distribution and the relevant emission intensity ratio can be used to label the local temperature of the luminescent centers.[40] Therefore, the radiation power density and the corresponding local temperature of the

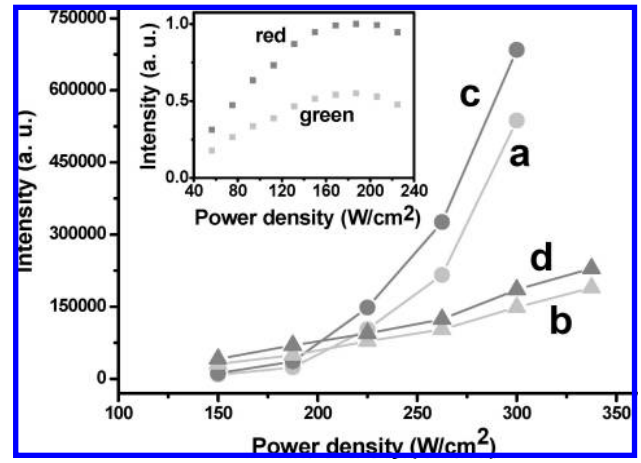

Figure 6. Green emissions at 525 and 545 nm ($^2H_{11/2}/^4S_{3/2} \rightarrow {}^4I_{15/2}$) of core (a) and core/shell (b) and 660 nm red emission ($^4F_{9/2} \rightarrow {}^4I_{15/2}$) of core (c) and core/shell (d) in high-power density regime. (Inset: Excitation power density dependence of the bulk counterpart emission). Here, the difference of Er^{3+} distribution between the two nanoparticle samples has been taken into account and the emission intensities of the two have been calibrated accordingly.

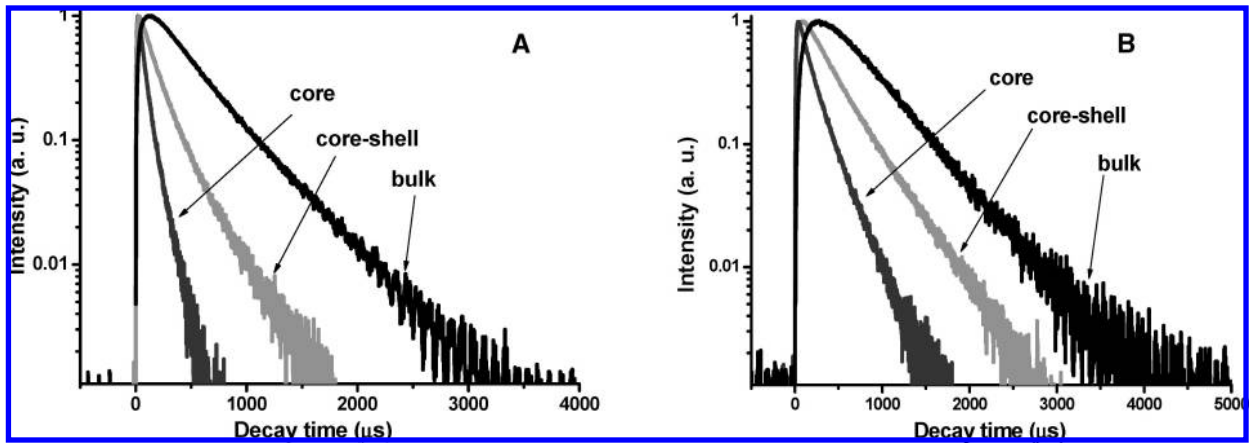

Figure 7. Temporal behavior of the green (A) and red (B) upconversion luminescence of the core, core/shell nanoparticles, and the bulk counterpart β-$NaYF_4$: Yb^{3+}, Er^{3+}.

TABLE 1: Excitation Power Density and the Corresponding Local Temperature of the Core and Core/Shell Nanoparticles

	low-power density				high-power density				
power density (W/cm^2)	60	90	120	150	187.5	225	262.5	300	337.5
core temperature (°C)	31.4	54.8	76.7	100.1	157.4	199.6	239.8	274.9	324.0
core/shell temperature (°C)	15.3	27.6	40.3	52.5	72.2	94.0	115.1	136.9	158.3

TABLE 2: Rise and Decay Times of Green and Red Upconversion Emissions of Core, Core/Shell Nanoparticles and the Bulk Counterpart

	$^4S_{3/2} \rightarrow {}^4I_{15/2}$ (green emission)			$^4F_{9/2} \rightarrow {}^4I_{15/2}$ (red emission)		
	core	core/shell	bulk	core	core/shell	bulk
rise time (μs)	7.0 ± 0.2	8.9 ± 0.4	40.0 ± 1.0	13.8 ± 0.4	29.3 ± 1.0	136.3 ± 0.1
decay time (μs)	$\tau_1 = 39.2 \pm 0.5$ (64.3%) $\tau_2 = 92.7 \pm 0.6$ (35.7%)	$\tau_1 = 128.7 \pm 0.9$ (78.8%) $\tau_2 = 302.4 \pm 2.1$ (21.2%)	$\tau = 406.3 \pm 1.5$	$\tau_1 = 87.5 \pm 1.6$ (48.0%) $\tau_2 = 222.4 \pm 1.1$ (52.0%)	$\tau_1 = 342.0 \pm 1.7$ (91.8%) $\tau_2 = 511.0 \pm 13.0$ (8.2%)	$\tau = 492.7 \pm 0.1$

radiation area can be related, as listed in Table 1. For core nanoparticles, it is clear that at low excitation the temperature of the samples is not higher than ~100 °C, whereas at high excitation the induced temperature can be as high as >300 °C, causing serious annealing of the samples. Here, a question may rise: why are the impacts on the upconversion spectrum not the same for the core and core/shell nanoparticles? To disentangle this, we have to consider the surface properties of the two samples. For core nanoparticles, the excitation energy of Yb^{3+} ions can efficiently excite the surface-related high vibrational frequency modes that will then be transferred to the low frequency lattice vibrational modes, lifting the temperature of the nanosystem. For the core/shell structure, on the contrary, the surface is separated by a shell from Yb^{3+} ions and the energy transfer channel of the excitation energy is thus blocked to a certain extent because the blocking effect depends on the quality of the shell. Thus, the temperature lifting in the core/shell nanoparticles will not be as apparent as that in the core nanoparticles under the same excitation power. The annealing naturally affects upconversion luminescence because it will lead to a more rigid structure, enhancing the upconversion emission (Figure 6). If the annealing effect is significant, the upconversion spectrum after will not be the same as that before, which is indeed the observation, that is when the excitation power density is >150 W/cm^2 (~100 °C) the upconversion spectrum cannot be recovered. In Figure 6, also the excitation power density dependence of the bulk sample is given. Clearly, its behavior is not in line with the nanoparticles in high-power region, where a slight dropdown of the intensities is observed. This might be related to energy transfer quenching, which seems not very important for the upconversion luminescence in the nanosystems.

At this end, we would like to discuss the time behavior of the upconversion spectra at the two excitation power levels. Figure 7 depicts the time evolution of the upconversion luminescence of the core and core/shell nanoparticles and the bulk samples. Rise and decay components are generally observed, similar to other reports.[41] Besides, all curves can be well fitted with the following equation,

$$I(t) = -Ae^{-t/\tau_r} + B_1e^{-t/\tau_1} + B_2e^{-t/\tau_2} \quad (2)$$

where A and B_1 and B_2 are all positive parameters. The assumption of one rise component is simply due to the limitation of the time resolution of the setup. In analysis of the curves, one has to realize that luminescence decay does not always represent the depopulation of the emissive state, and luminescence rise does not always represent the population of the emissive state as well. This is due to the fact that when a rise and a decay component coexist in luminescence kinetics, decay is always the longer one, even if the population is slower than the depopulation. *Upconversion luminescence of rare earth ions is just one of such examples*. Because the intermediate states mediate the upconversion process, for example $^4I_{11/2}$ and $^4I_{13/2}$ have much longer lifetimes relative to the final upconversion emission states, and for example $^4S_{3/2}$ (for green emission) and $^4F_{9/2}$ (for red emission), the rise components in our measurements are determined by the lifetimes of the latter states, whereas the intermediate states, that is $^4I_{11/2}$ and/or $^4I_{13/2}$, determine the decay components of the upconversion luminescence kinetics. Therefore, τ_1 and τ_2 in fact reflect mainly the nature of $^4I_{11/2}$ and $^4I_{13/2}$ states, and τ_r represents the lifetime of the $^4S_{3/2}$ or $^4F_{9/2}$.

The fitting results are given in Table 2. The decay time constants of the green emission ($^4S_{3/2} \rightarrow {}^4I_{15/2}$) lengthen from ~7 μs for the core to ~9 μs for the core/shell until ~40 μs for the bulk. Clearly, core/shell structure differs from the core in

removing the surface effect. This difference might be understood as follows: The core/shell structure separates in space from the surface from the luminescent centers, which can (i) to a certain extent block the excitation energy transportation to surface quenching centers, and (ii) recover the surface luminescent centers that are severely quenched in the core. Moreover, the multiphonon relaxation processes in the luminescent centers mediated by the surface-related organic high vibrational frequency modes will be different: the core/shell structure lengthens the distance between the luminescent centers and the vibrational modes, which will dim the interaction between the two and thus causes the nonradiative vibrational relaxation processes to be less efficient compared to the core sample.

The discussion above shall lead to the following conclusions: the lifetimes in core/shell nanoparticles are shorter than that of the bulk counterpart, although it is longer than that of the core nanoparticles and the actual lengthening depends on the shell thickness, and simultaneously n will decrease resulting from the evolution from linear-decay dominant to upconversion dominant. These are just the observations.

At the end, we would like to stress that in our experiments the samples were exposed to high-power radiation for as short as possible due to the fact that long-time annealing would result in a size increase of the nanoparticles. Therefore, the annealing process was far from complete to this extent. Even then, the annealing effect was very significant on the upconversion luminescence of the nanoparticles.

Conclusions

Steady-state and time-resolved spectroscopic studies are performed on one of the most efficient upconversion nanosystems − β-$NaYF_4$:Yb^{3+},Er^{3+} and β-$NaYF_4$:Yb^{3+},Er^{3+}@β-$NaYF_4$ core/shell nanoparticles. It is found that excitation power and surface properties, typically the high-frequency vibrational modes provided by the organic surfactants during the synthetic process, affect the luminescence upconversion dynamics.

Our results show that excitation power, once over a certain threshold, for example ∼150 W/cm^2 in this case, does have a non-negligible annealing effect. The surface-related high-frequency vibrations play an important role in the upconversion process as well as in the laser-induced annealing process in the core and core/shell nanoparticles. From luminescence kinetics analysis, it is clear that a large number of luminescent centers of the core nanoparticle are severely quenched but can be recovered by homogeneous coating. It is concluded that the upconversion emission spectrum, that is the ratio between the red and green emissions, can be greatly altered by excitation power density for core nanoparticles but not for core/shell nanoparticles.

Acknowledgment. This work was supported by NSFC of China (60771051, 60601015, 10674132, 10874179, and 20603035), and joint research program between C.A.S. of China and K.N.A.W. of The Netherlands.

References and Notes

(1) van de Rijke, F.; Zijlmans, H.; Li, S.; Vail, T.; Raap, A. K.; Niedbala, R. S.; Tanke, H. J. *Nat. Biotechnol.* **2001**, *19* (3), 273.
(2) Lim, S. F.; Riehn, R.; Ryu, W. S.; Khanarian, N.; Tung, C. K.; Tank, D.; Austin, R. H. *Nano Lett.* **2006**, *6* (2), 169.
(3) Wang, L. Y.; Li, Y. D. *Chem. Commun.* **2006**, *24*, 2557.
(4) Zhang, P.; Steelant, W.; Kumar, M.; Scholfield, M. *J. Am. Chem. Soc.* **2007**, *129*, 4526.
(5) Zhang, P.; Rogelj, S.; Nguyen, K.; Wheeler, D. *J. Am. Chem. Soc.* **2006**, *128*, 12410.
(6) Nyk, M.; Kumar, R.; Ohulchanskyy, T. Y.; Bergey, E. J.; Prasad, P. N. *Nano Lett.* **2008**, *8* (11), 3834.
(7) Menyuk, N.; Dwight, K.; Pinaud, F. *Appl. Phys. Lett.* **1972**, *21*, 159.
(8) Sommerdijk, J. L.; Bril, A. *Philips Tech. Rev.* **1974**, *34*, 1.
(9) Boyer, J. C.; Vetrone, F.; Cuccia, L. A.; Capobianco, J. A. *J. Am. Chem. Soc.* **2006**, *128* (23), 7444.
(10) Zhang, J.; Shade, C. M.; Chengelis, D. A.; Petoud, S. *J. Am. Chem. Soc.* **2007**, *129*, 14834.
(11) Schafer, H.; Ptacek, P.; Kompe, K.; Haase, M. *Chem. Mater.* **2007**, *19* (6), 1396.
(12) Wei, Y.; Lu, F.; Zhang, X.; Chen, D. *Chem. Mater.* **2006**, *18* (24), 5733.
(13) Yi, G.; Lu, H.; Zhao, S.; Ge, Y.; Yang, W.; Chen, D.; Guo, L. H. *Nano Lett.* **2004**, *4* (11), 2191.
(14) Mai, H. X.; Zhang, Y. W.; Sun, L. D.; Yan, C. H. *J. Phys. Chem. C* **2007**, *111* (37), 13721.
(15) Mai, H. X.; Zhang, Y. W.; Si, R.; Yan, Z. G.; Sun, L. D.; You, L. P.; Yan, C. H. *J. Am. Chem. Soc.* **2006**, *128* (19), 6426.
(16) Wang, L.; Li, Y. *Chem. Mater.* **2007**, *19* (4), 727.
(17) Li, C.; Quan, Z.; Yang, J.; Yang, P.; Lin, J. *Inorg. Chem.* **2007**, *46* (16), 6329.
(18) Zhao, J. W.; Sun, Y. J.; Kong, X. G.; Tian, L. J.; Wang, Y.; Tu, L. P.; Zhao, J. L.; Zhang, H. *J. Phys. Chem. B* **2008**, *112* (49), 15666.
(19) Stouwdam, J. W.; van Veggel, F. C. J. M. *Langmuir* **2004**, *20*, 11763.
(20) Hebbink, G. A.; Stouwdam, J. W.; Reinhoudt, D. N.; van Veggel, F. C. J. M. *Adv. Mater.* **2002**, *14*, 1147.
(21) Ermolaev, V. L.; Sveshnikov, E. B. *Russ. Chem. Rev.* **1994**, *63*, 905.
(22) Wang, Z. L.; Quan, Z. W.; Jia, P. Y.; Lin, C. K.; Luo, Y.; Chen, Y.; Fang, J.; Zhou, W.; O'Connor, C. J.; Lin, J. *Chem. Mater.* **2006**, *18*, 2030.
(23) Bu, W. B.; Hua, Z. L.; Chen, H. R.; Shi, J. L. *J. Phys. Chem. B* **2005**, *109* (30), 14461.
(24) Lehmann, O.; Kömpe, K.; Haase, M. *J. Am. Chem. Soc.* **2004**, *126* (45), 14935.
(25) Lü, Q.; Guo, F. Y.; Sun, L.; Li, A. H.; Zhao, L. C. *J. Phys. Chem. C* **2008**, *112* (8), 2836.
(26) Li, C. X.; Liu, X. M.; Yang, P. P.; Zhang, C. M.; Lian, H. Z.; Lin, J. *J. Phys. Chem. C* **2008**, *112* (8), 2904.
(27) Li, Q.; Gao, L.; Yan, D. S. *Chem. Mater.* **1999**, *11* (3), 533.
(28) Louis, C.; Roux, S.; Ledoux, G.; Dujardin, C.; Tillement, O.; Cheng, B. L.; Perriat, P. *Chem. Phys. Lett.* **2006**, *429*, 157.
(29) Bai, X.; Song, H. W.; Pan, G. H.; Liu, Z. X.; Lu, S. Z.; Di, W. H.; Ren, X. G.; Lei, Y. Q.; Dai, Q. L; Fan, L. B. *Appl. Phys. Lett.* **2006**, *88*, 143104.
(30) Zhu, L.; Liu, X. M.; Liu, X. D.; Li, Q.; Li, J. Y.; Zhang, S. Y.; Meng, J.; Cao, X. Q. *Nanotechnology* **2006**, *17*, 4217.
(31) Kömpe, K.; Borchert, H.; Storz, J.; Lobo, A.; Adam, S.; Möller, T.; Haase, M *Angew. Chem., Int. Ed.* **2003**, *42*, 5513.
(32) Yi, G. S.; Chow, G. M. *Chem. Mater.* **2007**, *19* (3), 341.
(33) Tyutyunnik, V. E.; Guloyan, Y. A. *Glass Ceram.* **2000**, *57*, 7–8.
(34) Yi, G. S.; Chow, G. M. *Adv. Funct. Mater.* **2006**, *16* (18), 2324.
(35) Pollnau, M.; Gamelin, D. R.; Lüthi, S. R.; Güdel, H. U. *Phys. Rev. B* **2000**, *61*, 3337.
(36) Liu, F.; Ma, E.; Chen, D. Q.; Yu, Y. L.; Wang, Y. S. *J. Phys. Chem. B* **2006**, *110* (42), 20843.
(37) Vetrone, F.; Boyer, J. C.; Capobianco, J. A.; Speghini, A.; Bettinelli, M. *J. Appl. Phys.* **2004**, *96*, 661.
(38) Bai, X.; Song, H. W.; Pan, G. H.; Lei, Y. Q.; Wang, T.; Ren, X. G.; Lu, S. Z.; Dong, B.; Dai, Q. L.; Fan, L. B. *J. Phys. Chem. C* **2007**, *111* (36), 13611.
(39) Yang, L. M.; Song, H. W.; Yu, L. X.; Liu, Z. X.; Lu, S. Z. *J. Lumin.* **2006**, *116*, 101.
(40) Wang, X.; Kong, X. G.; Yu, Y.; Sun, Y. J.; Zhang, H. *J. Phys. Chem. C* **2007**, *111* (41), 15119.
(41) Hehlen, M. P.; Frei, G.; Güdel, H. U. *Phys. Rev. B* **1994**, *50*, 16264.

JP9003399